International Journal of Engineering

Journal Homepage: www.ije.ir

Microstructure and Mechanical Properties of Polyamid 6/Acrylonitrile-butadiene Rubber Nanocomposites Fabricated by Friction Stir Process

A. Ghorbankhan, M. R. Nakhaei*

Facility of Mechanics and Energy, Shahid Beheshti University, Tehran, Iran

PAPER INFO

Paper history:
Received 10 August 2021
Received in revised form 05 September2021
Accepted 08 September2021

Keywords:
*Polyamid6/*Acrylonitrile-butadiene Rubber*/ Clay*
Nanocomposite
Modulus Strength
Eessential Work of Fracture
Response Surface Methodology

ABSTRACT

Thermoplastic elastomer (TPE) based on polyamid 6 (PA6)/ acrylonitrile-butadiene rubber (NBR) containing 5 wt % nanoclay (Closite 30B) have been prepared via friction stir process (FSP). In this study, the essential work of fracture (EWF) approach was employed to investigate the fracture behavior of PA6/NBR nanocompsites. Also, the modulus strength of specimens was modeled by response surface methodology (RSM), considering three input variables including rotational speed (ω), traverse speed (S), and shoulder temperature (T). Thus, a quadratic mathematical model between input variables (ω, S and T) and response (modulus strength) of PA6/NBR/clay nanocomposites was achieved. Moreover, the morphology of the PA6/NBR blends containing 5 wt % was investigated by x-ray diffraction (XRD), scanning electron microscopy (SEM), and transmission electron microscopy (TEM). The results show that a sample of PA6/NBR thermoplastic elastomer (TPE) containing 5 wt % nanoclay at maximum tensile strength exhibited the maximum specific essential work of fracture (w_e) and specific non-essential work of fracture (w_p). Also, the results of RSM method demonstrate that the optimum condition of the process including rotational speed (ω), traverse speed (S), and shoulder temperature (T) were 1200 rpm, 25mm/min, and 146℃, respectively. Thus, under optimum condition, maximum modulus strength of 658 MPa was obtained.

***doi**: 10.5829/ije.2021.34.10a.18*

1. INTRODUCTION

Thermoplastic elastomers (TPEs) are defined as a collection of copolymers (such as plastic and rubber) that consist of materials with both elastic (related to rubber phase) and strength (related to plastic phase) properties [1, 2]. They have a wide application in industry due to their ability to stretch, to moderate elongation and return to their near original shape, excellent thermal, mechanical, and chemical resistances [3, 4]. In recent years, a lot of articles reported on mechanical properties and fracture mechanisms of TPE blends [5-7]. The fracture toughness of PA6/NBR/Hallosite nanotube (HNTs) nanocomposite was investigated by Paran et al. [8]. Their results showed that the work of inner fracture zone (w_e) decreased with addition of HNTs into the PA6/NBR blend and, at the same time, the non-essential work of fracture (w_p) increased. Mahallati et al. [9] have investigated the effect of the NBR content and nanoclay loading on the microstructure and thermal behavior of PA6/NBR nanocomposites. They found that the storage modulus and oil resistance increased with the loading of the nanoclay. Paran et al. [10] have studied the effect of HNT on the mechanical and morphology properties of PA6/NBR blend. They concluded that the storage modulus, Young's modulus, and yield stress increased with increasing HNT content. The friction stir process is a new method for produce polymer nanocomposite [11]. The high rotational speed of the tool in this process leads to great shear stress in the process zone. The high shear stress leads to better nanofiller dispersion in the polymeric systems and improvement in the mechanical properties such as tensile, modulus strength, and fracture behavior. In this study, the effect of input variables such as shoulder temperature, rotational speed, and traverse speed on the total work of fracture and modulus strength of PA6/NBR/Clay are investigated by EWF and RSM approach, respectively. Also, the morphology of

*Corresponding Author Institutional Email: m_nakhaei@sbu.ac.ir (M. R. Nakhaei)

Please cite this article as: A. Ghorbankhan M. R. Nakhaei, Microstructure and Mechanical Properties of Polyamid 6/Acrylonitrile-butadiene Rubber Nanocomposites Fabricated by Friction Stir Process, IJE TRANSACTIONS A: Basics Vol. 34, No. 10, (October 2021) 2371-2378

PA6/NBR/Clay nanocomposites is studied by x-ray diffraction (XRD), transmission electron microscopy (TEM), and scanning electron microscopy (SEM).

2. Experimental design and procedure

2. 1. Materials To fabricate the specimens, polyamide 6 (PA6), nitrile butadiene rubber (NBR), and nanoclay (Cloisite 30B) were supplied from Kolon plastic co., Korea, Kumbo polymer Co., Korea, and Southern clay Co., USA, respectively. Chemical and physical characterizations of these materials are summarized in Table 1.

2. 2. TPE Nanocomposite Preparation The thermoplastic elastomer (TPE) nanocomposites based on PA6/NBR containing PA6 (70%) and NBR (30%) were prepared using a Brabender internal mixer at a process temperature of 230 ℃ with a screw speed of 80 rpm for 6 minutes. The workpiece sheets with 200×160×3.2 mm dimensions were achieved using a Mini Test Press operating at 130MPa.

2. 3. FSP Tool Johns describes many models to manufacture an FSP tool for polymers [11, 12]. Therefore, john's tool design is the model for the current tooling used at BYU. The FSP tool consists of two main functions: localized heating and material flow [13, 14]. Figure 1 shows the schematic of the FSP tools was used in this study. The FSP tool used in the study consist of a cylindrical threaded pin, a ball bearing, a heater, and a Teflon-coated shoulder (Figure 1).

To fabricate PA6/NBR/clay nanocomposite, a Deckel milling machine (M.S.T Co, Iran) was employed. The primary components were fixed on a milling machine, and a grove of 2.25 mm depth was machined in the middle of the workpiece. The nanoclay particles were placed in the groove, and they compressed. To obtain the height of the improvised nanoclay particle (h_n) in the groove, Equation (1) can be used:

$$h_n = \frac{A_g}{T_g . D_r} \quad (1)$$

where A_g and T_g are the cross-sectional area of groove and groove width, respectively. Also, D_r is the density ratio achieved by diving nanoparticles density by TPE composite density. Finally, the rotating tool along the groove moved to distribute nanoclay particles on the PA6/NBR blend.

In this study, the statistical and probabilistic methods of RSM with Box-Behnken three-level design is used to analyze the effect of input variables on mechanical properties. The ranges of input variables at three levels are shown in Table 2. Based on this design, fifteen experiments were carried to obtain the mathematical models, as shown in Table 3.

TABLE 1. Raw material properties used in nanocomposites

Material	Characteristics	Value	Units
PA6	Density	1.14	g/cm^3
	Melting point	220	℃
	Melt flow index (MFI)	31.4	g/10 min
	Mooney viscosity ML(1+4)125˚C	41	M
NBR	Bound Acrylonitrile	34	%
	Density	0.98	g/cm^3
Cloisite 30B	Modifier Concentration	90	Meq/100g
	Density	1.98	g/cm^3
	d-Spacing	18.4	Å

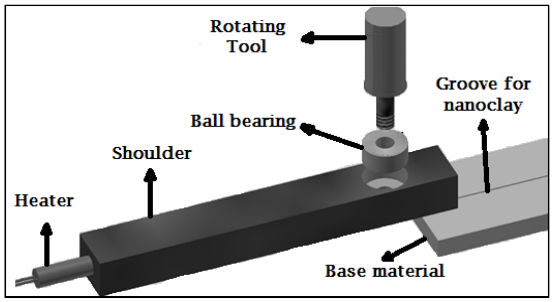

Figure 1. Schematics of friction stir process tool

2. 5. EWF Method One of the successful methods to investigate fracture behavior of nanocomposites is to use the essential work of fracture (EWF) method. This method is suitable for soft materials with low strength, such as polymers [15, 16]. In calculating fracture toughness of polymer nanocomposites, the EWF test, due to simple preparation of specimens and easy calculations has attracted considerable interest in academia and industries. In this method, to characterize the resistance to damage process occurring during tensile tests in outer fracture process zone (OPZ) and resistance to crack propagation in inner fracture process zone (IPZ), tensile test of double-edge notched tension (DENT) specimens with various values of ligament length (13, 15, 17 and 19 mm) were carried, based on ISO 293 protocol. Figure 2 demonstrates the schematic of the DENT specimens, FPZ, and OPZ [16, 17]. Using obtained load vs. displacement curves from tensile tests, EWF parameters can be achieved. The total work of fracture (W_f), which is calculated by the integral of F-D curves, consists of the applied work in a direction perpendicular to the ligament length (W_e) and plastic work in upper and lower areas of ligament length (W_p). The form of the formulation used for this parts is:

$$W_f = W_e + W_p \quad (2)$$

TABLE 2. The selected input variables and their limits

Parameters	Unit	Notations	Limits		
			–1	0	+1
Rotational speed	rpm	ω	800	100	1200
Traverse speed	mm/min	S	20	30	40
Shoulder temperature	℃	T	125	150	175

TABLE 3. Design matrix and the measured response

Run Order	ω (rpm)	S (mm/min)	T (℃)	Modulus Strength (MPa)
1	1200	20	150	645
2	1000	40	175	513
3	800	40	150	556
4	1200	30	175	613
5	1000	40	125	535
6	1000	20	125	543
7	800	30	125	533
8	800	20	150	549
9	1000	30	150	593
10	1200	30	125	626
11	1200	40	150	584
12	800	30	175	583
13	1000	30	150	595
14	1000	20	175	581
15	1000	30	150	597

Since the fracture toughness of polymer materials does not depend on the dimensions of specimens, Equation (2) can be rewritten by specific terms, as follows:

$$W_f = w_e.Lt + \beta L^2 t.w_p \quad (3)$$

$$w_f = \frac{W_f}{L} = w_e + \beta L.w_p \quad (4)$$

where $w_f, w_e, and\ w_p$ are specific work of fracture, specific essential work of fracture, and specific non-essential work of fracture, respectively. Also, β is the shape factor, and t is specimen thickness.

In other definition, the energy required to break, which is absorbed or consumed, can be defined by applied work in yielding (W_y) and necking + tearing (W_n) regions as follow:

$$W_f = W_y + W_n \quad (5)$$

By introducing Equation (3) into Equation (5), specific measurements of EWF parameters is written as follow:

$$w_f = (w_{e,y} + \beta L.w_{p,y}) + (w_{e,n} + \beta L.w_{p,n}) \quad (6)$$

where $w_{e,y}$, and $w_{e,n}$ are the specific yielding-related essential work of fracture and specific necking and tearing-related essential work of fracture, respectively. Also, $w_{p,y}$, and $w_{p,n}$ are specific plastic work of fracture in yielding and necking+ tearing zones, respectively [15, 17].

2. 6. Characterization The microstructures and phase morphology of the produced specimens were characterized using a Philips XL30 scanning electron microscope (Joel co., USA). For increasing the nanocomposite surface conductivity. Experimental measurements of nanoparticles distance were calculated by x-ray diffraction test. The aim of this test is to illustrate and compare the penetration of polyme chain between nanoclay layers in different samples of nanocomposites. For this work, using Philips X'Pert diffractometer with kα radiation of wavelength λ=1.540598 A°, the XRD curves of nanocomposites specimens were achieved. The dispersion of clay in the PA6/NBR blends was investigated using a transmission electron microscope (TEM) by a Philips EM208S at 100 kV. TEM samples were prepared by microtoming 80 nm thick using a diamond knife in an Ultracut Uct microtome (Leica Company, Austria). In order to investigate tensile properties of nanocomposites samples, tensile tests were performed using a Zuker tensile testing machine (Zwick Co., Germany). These experiments were performed at room temperature with crosshead speed of 1mm/min. Furthermore, the dimensions of specimens were determined based on the ASTM D256 standard [16]. Table 4 shows the average of three measurements of tensile tests for each run.

3. RESULTS

3. 1. Analysis of Variance (ANOVA) Depending on acceptable experimental data, analysis of variance (ANOVA) is a good technique for input variables screening which has the most effect on the output variables. In this method, the input variables with more F-value and less P-value (less 5% with 95% confidence level) have the most effect on the output variables. Therefore, they can be selected as the main variables with regard to their roles in the experimental data [2, 18]. The ANOVA table for the input and output variable are shown in Table 4. According to both columns F-value and P-value in Table 4, terms of shoulder temperature (T), rotational speed (ω), and traverse speed (S) as the linear effects are significant. Also, terms of quadratic and interaction effects of input variables such as ω^2, S^2, T^2 and ω×S, ω×T, S×T, can be regarded in the mathematical model. Due to the above results, the mathematical models for modulus strength are illustrated in Equations (7) and (8).

(a) In terms of coded factors:

$$\text{Modulus strength (MPa)} = 595 + 30.87\times\omega - 16.25\times S + 6.63\times T - 17\times\omega\times S - 15.75\times\omega\times T - 15\times S\times T + 17.13\times \omega^2 - 28.62\times S^2 - 23.38\times T^2 \quad (7)$$

(b) In term of actual factors:

$$\text{Modulus strength (MPa)} = -1218.85 + 0.025\times\omega + 33.05\times S + 16.43\times T - 0.0085\times\omega\times S - 0.0035\times\omega\times T - 0.06\times S\times T + 0.00042\times\omega^2 - 0.28\times S^2 - 0.037\times T^2 \quad (8)$$

3. 1. 1. Validation Equations (7) and (8) present the mathematical models of modulus strength with regard to 15 experimental tests. The accuracy and predictive capabilities of mathematical models can be assessed by comparing them with experimental results for various conditions [1, 11]. Therefore, the validation of mathematical models is investigated using three confirming experiments. The actual measurements, predicted values, and the percentage of error for three experiments with the new conditions are given in Table 5.

TABLE 4. ANOVA analysis for the modulus strength model

Source	Sum of Squares	df	Mean Square	F–Value	P-value
Model	19449.8	9	2161.0	87.3	< 0.0001
Rotational speed	7625.1	1	7626.1	306.1	< 0.0001
Traverse speed	2112.5	1	2112.5	85.3	0.0002
Shoulder	351.1	1	351.3	14.1	0.0131
ω×S	1156.0	1	1156.0	46.7	0.0010
ω×T	992.2	1	992.2	40.1	0.0014
S×T	90.0	1	900.0	36.3	0.0018
ω^2	1082.8	1	1082.8	43.7	0.0012
S^2	3025.4	1	3025.4	122.2	0.0001
T^2	2017.4	1	2017.4	81.5	0.0003
Residual	123.7	5	24.7		
Lack of Fit	115.7	3	38.5	9.65	0.0954
Pure Error	8.0	2	4.0		
Cor Total	19573.6	14			

TABLE.5. Validation of test results.

Run	Process parameters			Modulus Strength (MPa)
	ω	S	T	
1	1000	40	150	Actual: 550 Predict: 559 Error (%): 1.1
2	800	30	150	Actual: 581 Predict: 562 Error (%): 3.2
3	1200	20	175	Actual: 630 Predict: 661 Error (%): 4.9

According to the RSM method, the maximum and minimum modulus strength of PA6/NBR blends containing 5% wt nanoclay by different input variables values are given in Table 6. According to values of modulus strength in Table 6, the maximum modulus strength, which occurs at 1200 rpm (related to rotational speed), 25 mm/min (related to traversing speed), and 146℃ (related to shoulder temperature), is 658 MPa (TPO5-1 sample). Moreover, the minimum modulus strength of PA6/NBR/Clay nanocomposite is 521 MPa, which occurs at 800 rpm, 20 mm/min, and 130℃, respectively (TPO5-2 sample). Comparing mechanical properties of the TPO5-1 sample fabricated by FSP in this study with PA6/NBR/Clay produced by an internal mixer [9] shows that addition of nanoclay in the PA6/NBR blend increased the modulus strength of the nanocomposite from 378 to 658 and 630 MPa, respectively. Also, with addition of nanoclay to the PA6/NBR blend, the tensile strength of nanocomposites produce by the internal mixer decreased, whereas the tensile strength of FSP samples increased.

3. 2. Morphological Studies

3. 2. 1. XRD Analysis The corves of the XRD diffraction patterns for clay platelets and two samples of TPO5-1 and TPO5-2, as shown in Figure 2. Using calculating d-space from Bragg's law can be illustrated the rate of distribution of nanoclay in the matrix.

$$d = \frac{n\lambda}{2sin\theta} \quad (9)$$

where d, λ, and θ are the intergallery distance of clay, the x-ray wavelength, and angle related to the maximum point of the first peak, respectively. Also, n is the diffraction sequence [11]. As shown in Figure 2, the diffraction peak of neat clay appears at 2θ= 2.5°, corresponding to d_{001} basal spacing of 35.29 A° by Equation 11. In the XRD pattern of the TPO5-1 sample, the characteristic peak did not appear. This illustrates that the clay platelets in the matrix were exfoliated excellently in this sample. According to the researches, the size of clay particles on PP/EPDM thermoplastic elastomer reduced due to the higher rotational speed [1, 2]. On the other hand, the TPO5-2 sample exhibited an apparent peak at 2θ=2.3° (d= 38.36 A°). Thus, the observation above shows that the input variables (T, ω, and S) will determine the distribution quality of clay particles on PA6/NBR blends. According to the XRD results,

TABLE 6. Mechanical properties of TPO5-1 and TPO5-2 sample

Run	Process parameters			Tensile Strength (MPa)	Modulus Strength (MPa)	Impact Strength (j/m)
	ω	S	T			
TPO5-1	1200	25	146	32.9	658	69
TPO5-2	800	20	130	27.4	521	62

comparing X-ray diffraction patterns of the samples fabricated by FSP in this study and internal mixer [3, 9] shows that the correct choice of friction stir process parameters can have a great effect on nanoparticle dispersion on the polymer matrix.

3. 2. 2. SEM Figures 3 show the SEM micrographs of samples of TPO5-1 and TPO5-2. It was shown that the size of the NBR particles of the TPO5-1 sample is less than the TPO5-2 sample. Moreover, the amount of decrease in the size of NBR particles depends on the rotational speed values. Thus, as shown in Figure 3 that as rotating speed increases, shear stress increases, and the sizes of elastomer phases decreased [8, 10]. The size of the elastomeric phase in TPO5-2, observed as dark zones by scanning electron microscopy, was reduced with increasing rotational speed. Therefore, the decrease of NBR particles was well correlated with increasing the ω observed by SEM micrographs.

3. 2. 3. TEM The TEM micrographs of samples of TPO5-1 and TPO5-2 are illustrated in Figure 4. As shown in Figure 4, the PA6 and NBR phases are illustrated by gray and light areas, respectively. Also, the clay platelets on PA6/NBR blends are shown by dark lines. As shown in Figures 4a and 4b, the exfoliated rate of the TPO5-2 sample (Figure 4a) is better than the TPO5-1 sample (Figure 8b) on the PA6/NBR blend.

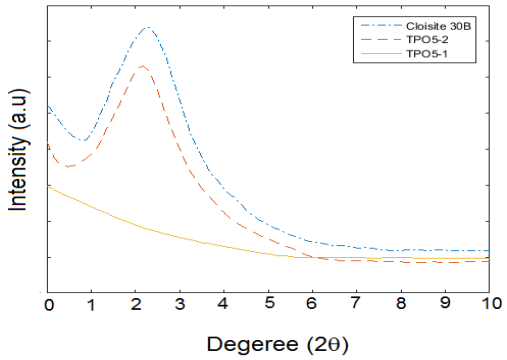

Figure 2. XRD Spectra of Closite 30B and PA6/NBR/Clay nanocomposites

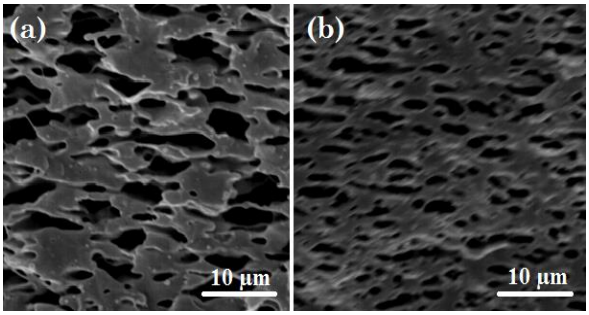

Figure 3. SEM micrograph of PA6/NBR nanocomposite (a) TPO5-2 and (b). TPO5-1

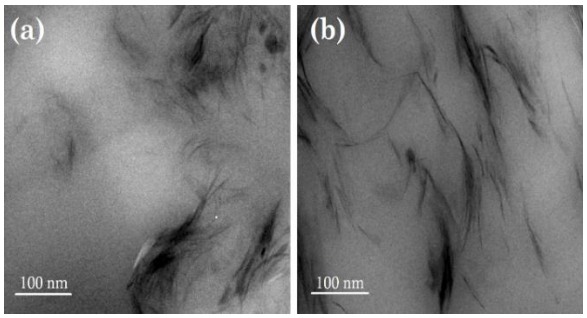

Figure 4. TEM micrograph of PA6/NBR nanocomposite (a) TPO5-2 and (b). TPO5-1

Following this reasoning, the potential energy for bond formation in interfaces of elastomeric and thermoplastic phases is great in TPO5-2 specimen compared to TPO5-1 specimen. On the other hand, an increase in modulus strength and fracture toughness of nanocomposites is dependent on the extent of exfoliation of nanoparticles in the matrix [11]. Thus, this result is in agreement with the fracture behavior and modulus strength of the specimens and could be an indication of comparatively stronger interactions between the clay nanoparticles and the PA6/NBR matrix in TPO5-2 sample.

3. 2. 4. EWF Test Due to the EWF test and DENT specimens with different ligament lengths (L), the load-displacement curves of PA6/NBR thermoplastic elastomers (TPEs) and TPO5-1 and TPO5-2 samples were illustrated in Figure 5. Figure 5a shows the load-displacement curve of the PA6/NBR blend containing 0% wt of nanoclay. Also, Figures 5b and 5c show the load-displacement curves of TPO5-1 and TPO5-2 samples, respectively. As indicated in Figure 5, the yielding parts in all samples have the same shapes, although this is not the same for all necking + tearing sections. Moreover, the integral of load-displacement curves for each sample increases with increasing ligament length. The maximum stress values (σ_{xax}) curves of PA6/NBR blend, TPO5-1, and TPO5-2 nanocomposites with different ligament lengths are illustrated in Figure 6. According to the ESIS stress criterion and Hills plasticity criterion, the maximum stress (σ_{xax}) values for each specimen should be in the range of 0.9-1.1 of the average of maximum stress. These criteria show that the fracture process of nanocomposite samples in the plane stress condition occurred. Therefore, Figure 4 shows that the application of the EWF theory in PA6/NBR/Clay nanocomposites is validated [2, 16].

EWF measurement for the yielding and necking + tearing sections are listed in Table 7. The results show that a sample of TPO5-2 exhibited the maximum specific essential work of fracture and specific non-essential work of fracture. This topic is clear thanks to good load transfer between matrix and nanoparticles due to better distribution of nanoparticles in the matrix, and less agglomeration compare with other samples [16].

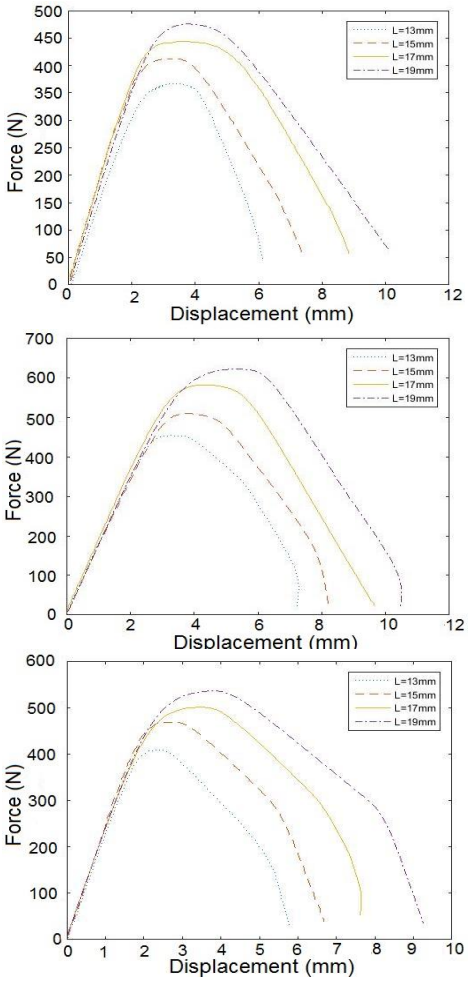

Figure 5. Force versus displacement curves for the three tested materials (a) PA6/NBR (b) TPO5-2 and (c).TPO5 – 1

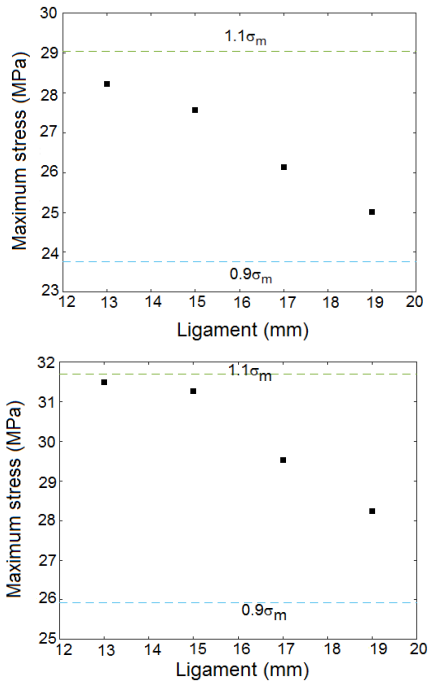

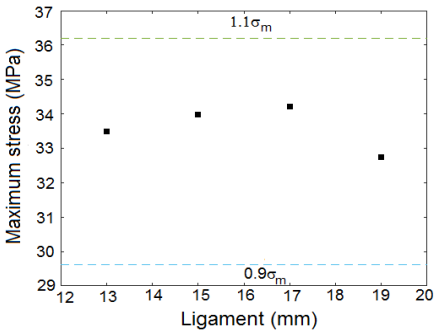

Figure 6. Maximum stress versus ligament length of (a) PA6/NBR (b) TPO5-2 and (c). TPO5-1

TABLE 7. The results of essential and non-essential work of fracture PA6/NBR, TPO5-1, and TPO5-2

Sample	W_e	βW_P	$W_{e,y}$	$\beta w_{p,y}$	$W_{e,n}$	$\beta w_{p,n}$
PA6/NBR	27.35	7.35	10.5	1	16.85	6.35
TPO5-1	12.8	8.1	6.2	2.1	6.6	6
TPO5-2	41.5	8.75	13.7	2.4	27.45	6.35

4. CONCLUSION

PA6/NBR nanocomposites containing 5% wt nanoclay Closite 30B were provided by friction stir process. The essential work of fracture (EWF) approach was used to investigate the fracture behavior of PA6/NBR/clay nanocomposites. Also, for modeling purposes and find the relationship between input variables and response (modulus strength), the RSM method was employed successfully. Moreover, using x-ray diffraction (XRD), transmission electron microscopy (TEM) scanning electron microscopy (SEM) were investigated the morphology of PA6/NBR blends containing 5 wt% nanoclay. The obtained result leads to the following conclusions.

1. Response surface methodology (RSM) is well applicable for modeling modulus strength of PA6/NBR/clay nanocomposite by mathematical models.
2. The modulus strength can be improved by increasing rotational speed in all encoded rang of the Box-Behnken design. Thus, the rotational speed has a the most effective on the modulus strength.
3. The results of the RSM method demonstrate that the optimum condition of the process was found to be at including rotational speed (ω), traverse speed (S), and shoulder temperature (T) of 1200 rpm, 25mm/min, and 146 ℃, respectively.
4. The total work of fracture increased with the presence of nanoclay. The sample of PA6/NBR TPE containing 5% wt nanoclay at maximum tensile strength exhibited the maximum specific essential work of fracture and the specific non-essential work of fracture.

5. The XRD results showed that the better distribution of nanoclay layers on PA6/NBR blend obtained for TPO5-2 sample.
6. SEM micrographs confirmed that amount of decrease in size of NBR particles depend on the rotational speed values, as well as, the higher rotational speed in FSP lead to higher shear stress and decreases size of NBR particles. Also, TEM images showed that an exfoliated and intercalated morphologies were obtained for the TPO5-2 sample.

5. REFERENCES

1. Nakhaei, M. and Naderi, G., "Modeling and optimization of mechanical properties of pa6/nbr/graphene nanocomposite using central composite design", ***International Journal of Engineering, Transactions C: Aspects***, Vol. 33, No. 9, (2020), 1803-1810. doi: 10.5829/IJE.2020.33.09C.15
2. Nakhaei, M.R., Mostafapour, A., Dubois, C., Naderi, G. and Reza Ghoreishy, M.H., "Study of morphology and mechanical properties of pp/epdm/clay nanocomposites prepared using twin-screw extruder and friction stir process", ***Polymer composites***, Vol. 40, No. 8, (2019), 3306-3314. doi: 10.1002/PC.25188
3. Yudhanto, F., Jamasri, J., Rochardjo, H. S. B., and Kusumaatmaja, A., "Experimental Study of PVA Nanocomposite Film Reinforced by Cellulose Nanofibers from Agave Cantala" I***nternational Journal of Engineering, Transactions A: BAsics,*** Vol. 34, No. 4, (2021) 987-998. doi: 10.5829/IJE.2021.34.04A.25
4. Qiu, Y., Wang, J., Wu, D., Wang, Z., Zhang, M., Yao, Y. and Wei, N., "Thermoplastic polyester elastomer nanocomposites filled with graphene: Mechanical and viscoelastic properties", ***Composites Science and Technology***, Vol. 132, (2016), 108-115. doi: 10.1016/J.COMPSCITECH.2016.07.005
5. Azdast, T. and Hasanzadeh, R., "Tensile and morphological properties of microcellular polymeric nanocomposite foams reinforced with multi-walled carbon nanotubes", ***International Journal of Engineering, Transactions C: Aspects***, Vol. 31, No. 3, (2018), 504-510. doi: 10.5829/IJE.2018.31.03C.14
6. Rashahmadi, S., Mosalman, S. and Hasanzadeh, R., "The effect of tio2 nanoparticles on mechanical properties of poly methyl methacrylate nanocomposites (research note)", ***International Journal of Engineering, Transactions B: Applications***, Vol. 30, No. 5, (2017), 807-813. doi: 10.5829/IDOSI.IJE.2017.30.05B.22
7. Ghasemi, F.A., Niyaraki, M.N., Ghasemi, I. and Daneshpayeh, S., "Predicting the tensile strength and elongation at break of pp/graphene/glass fiber/epdm nanocomposites using response surface methodology", ***Mechanics of Advanced Materials and Structures***, Vol. 28, No. 10, (2021), 981-989. doi: 10.1080/15376494.2019.1614702
8. Paran, S., Naderi, G., Ghoreishy, M. and Dubois, C., "Essential work of fracture and failure mechanisms in dynamically vulcanized thermoplastic elastomer nanocomposites based on pa6/nbr/xnbr-grafted hnts", ***Engineering Fracture Mechanics***, Vol. 200, (2018), 251-262. doi: 10.22063/JIPST.2020.1732
9. Mahallati, P., Arefazar, A. and Naderi, G., "Thermoplastic elastomer nanocomposites based on pa6/nbr", ***International Polymer Processing***, Vol. 25, No. 2, (2010), 132-138. doi: 10.3139/217.2311
10. Paran, S.R., Naderi, G. and Ghoreishy, M.R., "Effect of halloysite nanotube on microstructure, rheological and mechanical properties of dynamically vulcanized pa6/nbr thermoplastic vulcanizates", ***Soft Materials***, Vol. 14, No. 3, (2016), 127-139. doi: 10.1080/1539445X.2016.1157694
11. Nakhaei, M., Naderi, G. and Mostafapour, A., "Effect of processing parameters on morphology and tensile properties of pp/epdm/organoclay nanocomposites fabricated by friction stir processing", ***Iranian Polymer Journal***, Vol. 25, No. 2, (2016), 179-191. doi: 10.1007/S13726-015-0412-6
12. Zinati, R.F. and Razfar, M.R., "Finite element simulation and experimental investigation of friction stir processing of polyamide 6", ***Proceedings of the Institution of Mechanical Engineers, Part B: Journal of Engineering Manufacture***, Vol. 229, No. 12, (2015), 2205-2215. doi: 10.1177/0954405414546705
13. Goli Bidgoli, M., Ranjbaran, A., Mirzavand, K., Shajari, Y., Seyedraoufi, Z. S., Porhonar, M., "Investigation of Carbon Fiber Reinforced Polymer Composite Welding with a New Tool in Friction Stir Welding Method" I ***International Journal of Engineering, Transactions C: Aspects***, Vol. 32, No. 6, (2019) 860-865. doi: 10.5829/IJE.2019.32.06C.09
14. Huang, Y., Meng, X., Xie, Y., Wan, L., Lv, Z., Cao, J. and Feng, J., "Friction stir welding/processing of polymers and polymer matrix composites", ***Composites Part A: Applied Science and Manufacturing***, Vol. 105, (2018), 235-257. doi: 10.1016/J.COMPOSITESA.2017.12.005
15. Hafiz, T., "Influence of temperature and moisture on the compressive strength of carbon fiber reinforced polymers", ***International Journal of Engineering, Transactions B: Applications***, Vol. 33, No. 5, (2020), 916-922. doi: 10.5829/IJE.2020.33.05B.24
16. Khodabandelou, M., Aghjeh, M.K.R. and Mazidi, M.M., "Fracture toughness and failure mechanisms in un-vulcanized and dynamically vulcanized pp/epdm/mwcnt blend-nanocomposites", ***RSC Advances***, Vol. 5, No. 87, (2015), 70817-70831. doi: 10.1039/C5RA12087J
17. Bárány, T., Czigány, T. and Karger-Kocsis, J., "Application of the essential work of fracture (ewf) concept for polymers, related blends and composites: A review", ***Progress in Polymer Science***, Vol. 35, No. 10, (2010), 1257-1287. doi: 10.1016/J.PROGPOLYMSCI.2010.07.001
18. Sahith Reddy, S., "Optimization of calcined bentonite caly utilization in cement mortar using response surface methodology", ***International Journal of Engineering, Transactions A: BAsics***, Vol. 34, No. 7, (2021), 1623-1631. doi: 10.5829/IJE.2021.34.07A.07

Persian Abstract

چکیده

ترموپلاستیک الاستومرهای بر پایه پلی آمید 6/ نیتریل بوتادین رابر (PA6/NBR) شامل 5 ٪ وزنی نانو ذرات خاک رس با فرایند اصطکاکی اغتشاشی (FSP) ساخته شد. در این تحقیق از کار ضروری شکست (EWF) برای بررسی رفتار شکست ترکیب های PA6/NBR با 0% و 5% درصد وزنی خاک رس استفاده شد.همچنین مدول کششی نمونه ها با استفاده از روش پاسخ سطح (RSM) مدلسازی شد که سه پارامتر ورودی شامل سرعت چرخشی ابزار (ω)، سرعت خطی (S) و دمای شولدر (T) مورد نظر قرار گرفت. بنابراین یک معادله ریاضی درجه دوم بین متغییرهای ورودی و پاسخ بدست آمد. علاوه بر این، ریز ساختار ترکیب PA6/NBR شامل 5% نانو ذرات خاک رس با پراش اشعه ایکس (XRD)، میکروسکوپ الکترونی روبشی (SEM) و میکروسکوپ الکترونی عبوری (TEM) مورد بررسی قرار گرفت. نتایج نشان می دهد که نمونه دارای بیشترین استحکام کششی دارای بیشترین کار ضروری و کار غیر ضروری شکست است. همچنین نتایج حاصل از RSM نشان داد که بیشترین مدول کششی زمانی بدست خواهد آمد که سرعت چرخشی، سرعت خطی و دمای شولدر ابزار به ترتیب برابر با 1200 rpm، 25 mm/min و 146 °C است که در این شرایط بهینه، مدول کششی برابر 658 MPa بدست خواهد.